A potential target for liver cancer management, lysophosphatidic acid receptor 6 (LPAR6), is transcriptionally up-regulated by the NCOA3 coactivator

Received for publication, June 21, 2019, and in revised form, November 25, 2019 Published, Papers in Press, December 30, 2019, DOI 10.1074/jbc.RA119.009899

Xuan Zheng[‡§], Yinghui Jia[§], Lei Qiu[§], Xinyi Zeng[§], Liangliang Xu[¶], Mingtian Wei[‖], Canhua Huang[§], Cong Liu[**], Liangyi Chen[‡1], and Junhong Han[§2]

*From the [‡]State Key Laboratory of Membrane Biology, Beijing Key Laboratory of Cardiometabolic Molecular Medicine, Institute of Molecular Medicine, Peking University, Beijing 100871, China, the [§]Department of Abdominal Oncology, State Key Laboratory of Biotherapy and Cancer Center, West China Hospital, Sichuan University, and Collaborative Innovation Center for Biotherapy, Chengdu 610041, China, the [¶]Department of Liver Surgery, West China Hospital, Sichuan University, Chengdu 610041, China, the [‖]Department of Gastrointestinal Surgery, West China Hospital, Sichuan University and Collaborative Innovation Center for Biotherapy, Chengdu 610041, China, and the **Department of Paediatrics, Key Laboratory of Birth Defects and Related Diseases of Women and Children (Ministry of Education), West China Second University Hospital, Sichuan University, Chengdu 610041, China*

Edited by John M. Denu

Lysophosphatidic acid receptor 6 (LPAR6) is a G protein–coupled receptor that plays critical roles in cellular morphology and hair growth. Although LPAR6 overexpression is also critical for cancer cell proliferation, its role in liver cancer tumorigenesis and the underlying mechanism are poorly understood. Here, using liver cancer and matched paracancerous tissues, as well as functional assays including cell proliferation, quantitative real-time PCR, RNA-Seq, and ChIP assays, we report that LPAR6 expression is controlled by a mechanism whereby hepatocyte growth factor (HGF) suppresses liver cancer growth. We show that high LPAR6 expression promotes cell proliferation in liver cancer. More importantly, we find that *LPAR6* is transcriptionally down-regulated by HGF treatment and that its transcriptional suppression depends on nuclear receptor coactivator 3 (NCOA3). We note that enrichment of NCOA3, which has histone acetyltransferase activity, is associated with histone 3 Lys-27 acetylation (H3K27ac) at the *LPAR6* locus in response to HGF treatment, indicating that NCOA3 transcriptionally regulates LPAR6 through the HGF signaling cascade. Moreover, depletion of either *LPAR6* or *NCOA3* significantly inhibited tumor cell growth *in vitro* and *in vivo* (in mouse tumor xenograft assays), similar to the effect of the HGF treatment. Collectively, our findings indicate an epigenetic link between LPAR6 and HGF signaling in liver cancer cells, and suggest that LPAR6 can serve as a biomarker and new strategy for therapeutic interventions for managing liver cancer.

During the past years, multiple targets were characterized to develop new drugs for liver cancer; nevertheless, many of these drugs failed in Phase III trials (1, 2). Currently, sorafenib is the only first-line drug in liver cancer treatment, yet the five-year survival rate remains low. Therefore, finding new targets and developing specific drugs is still an urgent issue (3–5). Hepatocyte growth factor (HGF)[3] is a multipotent cytokine secreted by mesenchymal cells, acting mainly on epithelial-derived cells (6). It binds to the c-Met receptor, activating tyrosine kinase cascade to regulate cellular physiological properties that endow an important role in angiogenesis, tissue regeneration, and tumorigenesis (7–10). The abnormal HGF/MET signaling mediated by Met receptor mutation, cross-talk of Met with EGFR/ERBB2/IGF1R, and the promoting effect to angiogenesis all make HGF an enhancer of tumorigenesis (11–14). Surprisingly, HGF expression is lower in some liver tumor tissues compared with paracancerous tissues (15–17). We and others have previously reported that HGF can specifically inhibit the growth of HepG2 cells through ERK activation (18–21). Although some potential targets and pathways were identified, a detailed regulatory mechanism and *in vivo* evidence of this interesting phenomenon remains poorly defined (22–24).

Lysophosphatidic acid receptor 6 (LPAR6), a G protein–coupled receptor that is highly expressed in epithelial cells and hair follicles, mediates cAMP accumulation and Rho-dependent cellular morphological changes (25, 26). Some mutations in this gene have been found to cause hypotrichosis (27, 28). Surprisingly, both in liver cancer cell lines and patient tumors, LPAR6 positively correlates with proliferative activity (29, 30).

This work was supported by The National Key Research and Development Program of China Grant 2018YFC1312300, National Natural Science Foundation of China Grant NSFC 81672782, Fundamental Research Funds for the Central Universities Grant 20822041A4065, Sichuan Science and Technology Program Grant 2018JY0018, the 1·3·5 Project for Disciplines of Excellence, West China Hospital Grant ZYGD18003, and the Sichuan University (to J. H.). The authors declare that they have no conflicts of interest with the contents of this article.

This article contains Figs. S1–S4.

[1] To whom correspondence may be addressed. E-mail: lychen@pku.edu.cn.
[2] To whom correspondence may be addressed. E-mail: hjunhong@scu.edu.cn.

[3] The abbreviations used are: HGF, hepatocyte growth factor; NCOA3, nuclear receptor coactivator 3; LPAR6, lysophosphatidic acid receptor 6; HAT, histone acetyltransferase; IHC, immunohistochemistry; NT, scrambled shRNA; c-MET, MET proto-oncogene; CBP, CREB-binding protein; p300, E1A-binding protein P300; IRS, immunoreactivity score; IOD, integrated optical density; qPCR, quantitative PCR; FPKM, fragments per kilobase of exon per million fragments mapped; ERK, extracellular signal-regulated kinase; CREB, cAMP-response element-binding protein; GAPDH, glyceraldehyde-3-phosphate dehydrogenase.

However, the underlying molecular mechanism is still largely unknown.

NCOA3 is a member of the steroid receptor coactivator family (31). NCOA3 has intrinsic histone acetyltransferase (HAT) activity and contains two transcriptional activation domains that recruit CBP/p300 and histone methyltransferases (32–34). Previous studies have revealed that NCOA3 expression is elevated in multiple tumor types (33). Also that NCOA3 overexpression contributes to cancer initiation, metastasis, and chemoresistance by mostly activating signaling cascades leading to uncontrolled proliferation (35). However, no correlation between NCOA3 and LPAR6 has been found so far.

In this study, we aimed to understand the role of LPAR6 in liver tumorigenesis and the underlying mechanism for LPAR6 regulation. We found that LPAR6 was overexpressed in liver tumor tissues and contributed to HepG2 cell proliferation. Moreover, HepG2 cells treated with HGF showed LPAR6 down-regulation in an NCOA3-dependent manner. More importantly, loss of either LPAR6 or NCOA3 significantly inhibited tumor cell growth *in vitro* and *in vivo*. Chromatin immunoprecipitation (ChIP) assay revealed that NCOA3 enrichment was closely correlated with the H3K27ac level at the *LPAR6* locus in response to HGF treatment, indicating that NCOA3 transcriptionally regulates *LPAR6* as part of the HGF signaling cascade. Moreover, HGF demonstrated strong inhibition toward HepG2-developed xenograft tumor growth, providing promising evidence for *in vivo* usage of HGF in treating liver cancer. Our study reveals a novel epigenetic regulatory mechanism for HGF inhibition on HepG2 cell growth and provides *in vivo* evidence for the therapeutic potential of HGF and its downstream targets.

Results

LPAR6 is highly expressed in liver cancer and closely related to liver cancer patient survival

To determine the role of LPAR6 in hepatocellular carcinoma, we analyzed LPAR6 expression in liver cancer and matched paracancerous tissues. Immunostaining of liver specimens in IRS (immunoreactivity score) between tumors and paracancerous tissues is based on the intensity of LPAR6 staining. Image-Pro Plus 6.0 was used for further IRS analysis. Both histochemistry and integrated optical density (IOD)/area of LPAR6 positivity in images indicated significantly higher expression of LPAR6 in tumors (Fig. 1, *A* and *B*). Moreover, survival analysis of 63 patients revealed a negative correlation between LPAR6 expression and patient prognosis (Fig. 1*C*). Taken together, these results suggest that highly expressed LPAR6 in liver cancer patients may promote tumor growth and lead to poor survival.

To further confirm our findings, we verified LPAR6 expression by analyzing data from the TCGA database. We found that LPAR6 was highly expressed in liver cancer ($p < 0.0001$) compared with normal liver tissue (Fig. 1*D*). Ethnic analysis revealed a significant increase in LPAR6 expression in Caucasian and Asian liver cancer samples (Fig. 1*E*). Both tumor grade and stage showed that LPAR6 expression increased in tumor compared with paracancerous tissue (Fig. 1, *F* and *G*). In addition, the ENCODE database showed that LPAR6 transcription was also significantly increased in HepG2 cells compared with normal liver cells (Fig. 1*H*). Studies show that proto-oncogene *c-Myc* or *RhoA* directly link to liver cancer (36, 37). Thus, we analyzed their correlation with *LPAR6* in liver cancer. Pearson correlation coefficient analysis showed a strong correlation between *LPAR6* and *c-Myc* or *RhoA* expression levels (Fig. 1*I*), suggesting that LPAR6 may play a key role in carcinogenesis of liver cancer and may be a potential therapeutic target.

LPAR6 promotes HepG2 cell proliferation

To test whether LPAR6 does play a role in liver carcinogenesis, we knocked down LPAR6 with shRNA (Fig. 2*A*) and performed a proliferation activity assay using EdU staining. We found that EdU-positive cells were remarkably reduced with *LPAR6* knockdown (Fig. 2*B*). Clonogenicity was also diminished in *LPAR6* knockdown cells (Fig. 2, *C* and *D*). In addition, *LPAR6* knockdown significantly attenuated HepG2 and Huh7 cell proliferation (Fig. 2, *E* and *F*), which may be due to cell cycle arrest because LPAR6 depletion caused G1 phase arrest (Fig. 2*G*). More importantly, LPAR6 overexpression significantly promoted HepG2 and Huh7 cell proliferation (Fig. 2, *H* and *I*). Together, these data indicate that LPAR6 is a key factor that promotes HepG2 cell growth.

HGF inhibits HepG2 proliferation by down-regulating LPAR6

Because HGF can specifically inhibit HepG2 cell proliferation (19, 20), we sought to investigate the underlying mechanisms. We first tested the proliferation of HepG2 cells cultured with 50 ng/ml of HGF for 5 days, and found that HGF indeed inhibited HepG2 proliferation and clonogenicity (Fig. 3, *A*–*C*). To further test the anti-tumor effect of HGF, we cultured HepG2 cells with HGF at a final concentration of 50 ng/ml for 4 days and then implanted cells into the dorsal ventral skin of nude mice. The tumor volume was monitored for 30 days, and the tumor size in the HGF-treated group was much smaller than that in the control group (Fig. 3*D*). IHC results revealed that LPAR6 expression was reduced in HGF-treated tumor tissues (Fig. 3*E*). These results suggest that LPAR6 may be involved in the anti-proliferative effect of HGF in cancer.

To explore genes potentially involved in HGF-induced HepG2 proliferation inhibition, we performed whole-genome transcriptome analysis by RNA-seq. For the convenience of sequencing data analysis, we set T to represent the HGF-treated group and C as untreated cells. To study the differentially expressed genes shared between the replicates, we divided the experimental data into three groups (T1 *versus* C1, T2 *versus* C2, T1 + T2 *versus* C1 + C2) and performed differential gene expression analyses between the groups. We found 723 differentially expressed genes between HGF-treated and untreated cells (T1 + T2 *versus* C1 + C2) and 653 differentially expressed genes shared between the three groups (Fig. 3*F*). Among the significantly changed genes, 587 genes were up-regulated and 136 genes were down-regulated by HGF in T1 + T2 *versus* C1 + C2 (Fig. 3*G*). Interestingly, *LPAR6* was transcriptionally down-regulated by HGF (Fig. 3*H*), and the reduction was also confirmed by immunoblotting and quantitative real-time PCR

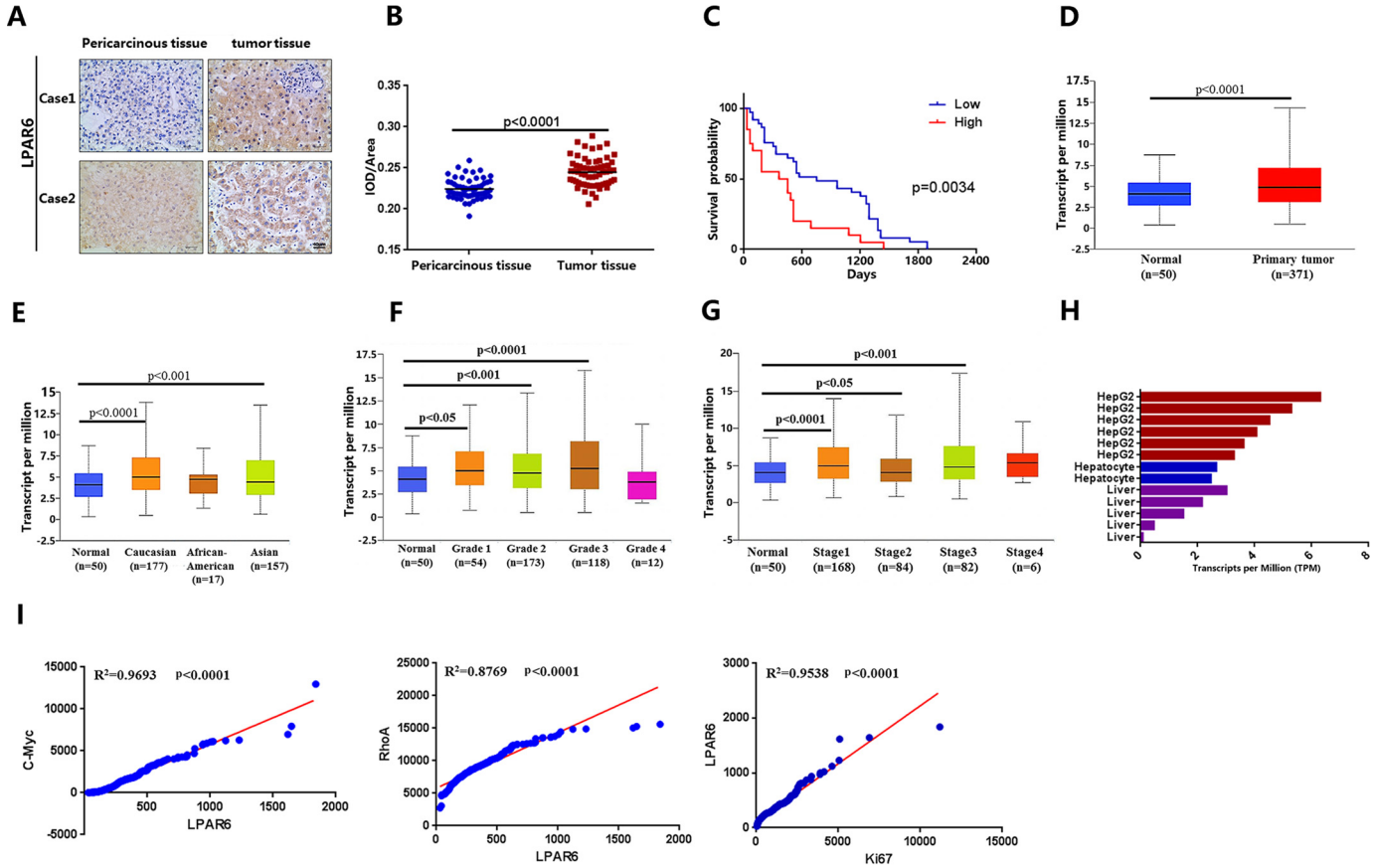

Figure 1. LPAR6 serves as a potential liver cancer target. *A,* representative IHC detection of LPAR6 in human liver cancer and paracancerous tissues. *Brown* stained for positive cells. *B,* immunostaining of LPAR6 was scored with IOD/area and analyzed in IRS. *C,* Kaplan-Meier plots showing the survival of liver cancer patient of LPAR6 expression. Log-rank test shows statistically significant differences between high and low groups ($p = 0.0034$). According to the LPAR6 optical density of IHC specimens and survival status events (0 for survival, 1 for death), the cutoff value was obtained by ROC curve analysis. IHC specimens were divided into high and low expression groups by cutoff value. *D,* analysis of the *LPAR6* expression level between normal liver tissues *versus* liver cancer tissues. Data represent mean ± S.D. Significance of expression level differences was determined using Student's *t* test ($p < 0.0001$). *E–G,* expression level of *LPAR6* in different race, grade, and tumor stage on the basis of liver cancer compared with normal liver tissues. Data represent mean ± S.D. Significance of expression level differences was determined using Student's *t* test ($p < 0.05$, $p < 0.001$, and $p < 0.0001$). *H,* comparison of *LPAR6* transcription levels in HepG2, hepatocytes, and normal liver cells of donor. *TPM*, transcripts per million reads. *I,* linear regression analyses of *LPAR6*, *C-Myc*, and *RhoA*, respectively. Pearson correlation coeffients show strong correlation of expression level between *LPAR6* and *c-Myc* or *RhoA*. Raw data were obtained from OncoLnc database.

(qPCR) (Fig. 3, *I* and *J*). Immunofluorescence staining with LPAR6 antibody showed weaker fluorescence signals in HGF-treated HepG2 cells compared with untreated cells (Fig. 3*K*). These results indicate that LPAR6 is a key downstream gene regulated by HGF in liver cancer. Studies implied that HGF inhibited HepG2 cell growth through the MEK/ERK signaling pathway, thus we tested whether MEK inhibitor U0126 blocked HGF-induced LPAR6 decrease. Indeed, U0126 rescued LPAR6 expression in HepG2 cells treated with HGF (Fig. 3*L*), indicating the regulation of LPAR6 expression by HGF was also mediated by the MEK/ERK signaling pathway. In addition, LPAR6 overexpression stimulated cell proliferation, suggesting that LPAR6 could partially rescue HGF-induced HepG2 cell proliferation arrest (Fig. 3*M*). These results further support that LPAR6 is important for liver cancer growth.

H3K27ac enrichment is elevated at LPAR6 promoter in HepG2 cells

To address the underlying mechanism regarding how HGF regulate LPAR6 expression, we mainly focused on the epigenetic regulation on *LPAR6* transcription. First, we analyzed the profile of histone modifications at *LPAR6* locus. Compared with normal donor hepatocytes, H3K27ac (active transcription marker) was significantly enriched in the promoter region of *LPAR6* in HepG2 cells, whereas H3K9ac (active transcription marker), H3K9me3 and H3K27me3 (both are suppressive transcription markers) had slight differences (Fig. 4*A*, Fig. S1). Therefore, we hypothesized that certain histone acetylation-modifying enzymes or co-activators might be involved in *LPAR6* regulation. To identify these regulators, we performed qPCR targeting all histone acetylation modifiers and found that *NCOA3* transcription was significantly up-regulated in HepG2 compared with liver cell line LO2 (Fig. 4*B*). Thus, we speculated that NCOA3 might serve as an epigenetic regulator of *LPAR6* transcription. Western blotting results indicated that LPAR6 expression was indeed down-regulated with *NCOA3* knockdown (Fig. 4*C*).

To verify whether NCOA3 also plays a role in promoting cancer growth, we knocked down *NCOA3* in HepG2 cells and performed functional analyses. Cell proliferation measured by

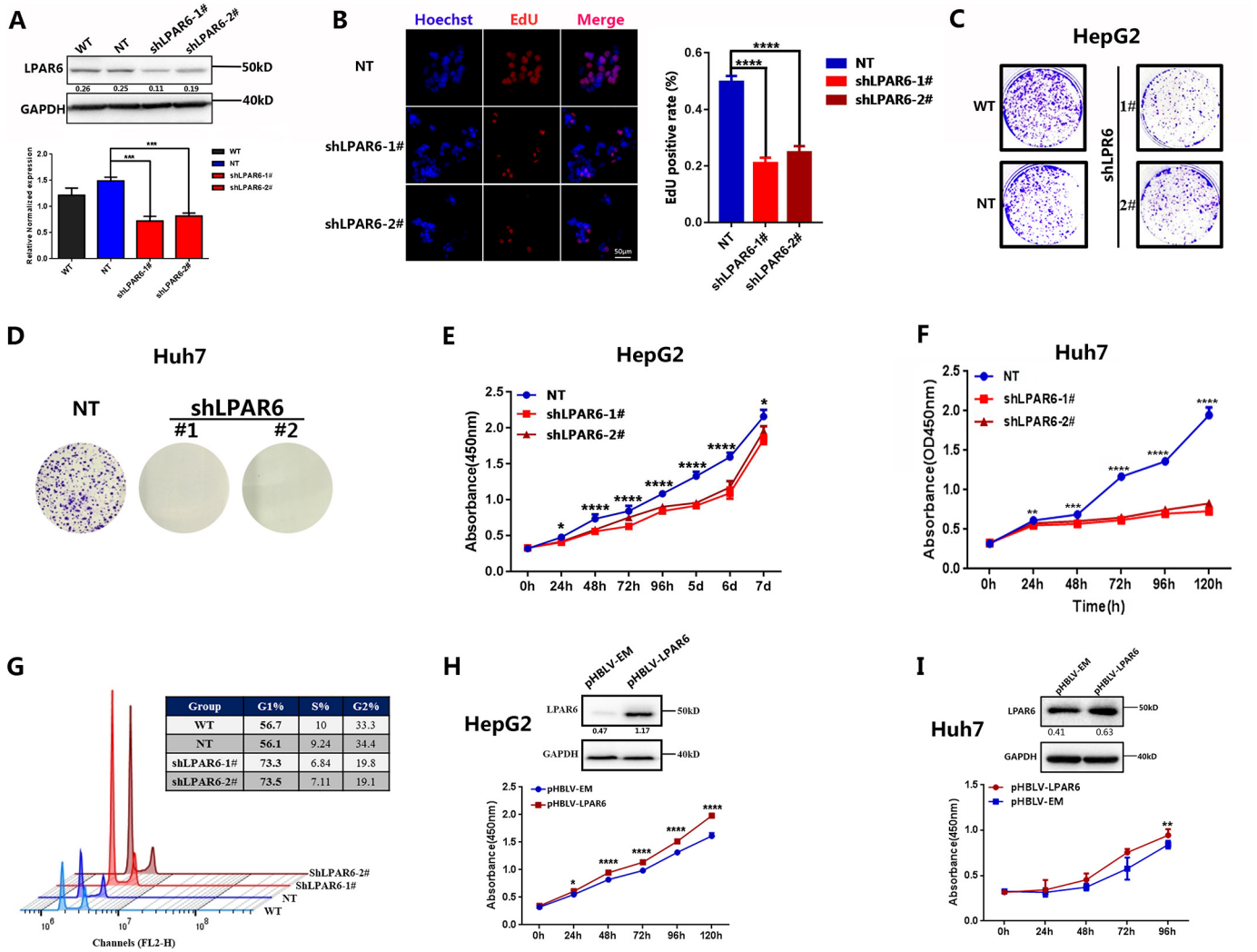

Figure 2. LPAR6 promotes HepG2 cell proliferation whereas HGF suppresses it. *A,* knockdown efficiency of *LPAR6*-shRNA and *LPAR6* expression levels evaluated by qPCR and normalized to the housekeeping gene, *GAPDH*. *WT*, cells without transfection. *NT*, cells transfected with scrambled shRNA. sh*LPAR6*, cells transfected with *LPAR6* shRNA. *Error bars* represent the S.D. from at least three independent biological replicates (***, $p < 0.001$). *B,* EdU staining indicates increased cell mitosis activity with knockdown of *LPAR6* using *LPAR6*-shRNA (sh*LPAR6*), and scrambled shRNA (*NT*) was used as control. *Left panel*, *red* represents EdU staining for replicated DNA; *blue* represents Hoechst staining for cell nucleus; the *merged lane* shows colocalization. *Scale bar* = 50 μm. *Right panel*, quantification (percentage of EdU positive cells) of the *left panel*. Data represent mean ± S.D. from at least three independent assays. ****, $p < 0.0001$. *C* and *D,* colony formation of (*C*) HepG2 and (*D*) Huh7 cells with or without *LPAR6* depletion; representative images shown here are selected from three independent experiments. *E* and *F,* cell-proliferation assay of (*E*) HepG2 and (*F*) Huh7 cells with or without *LPAR6* knockdown. *NT*, cells transfected with scrambled shRNA served as control. Data represents mean ± S.D. from three independent experiments. ****, $p < 0.0001$. *G,* FACS assay showing cell cycle distribution of HepG2 cells with or without *LPAR6* knockdown. Data represents one of three independent experiments. The statistical differences shown in this figure were determined by Student's *t* test. *H* and *I,* overexpression of *LPAR6* with (pHBLV-LPAR6) promoted (*H*) HepG2 and (*I*) Huh7 cell proliferation compared with control (pHBLV-EM) cells. Data represents mean ± S.D. from three independent experiment: **, $p < 0.01$; ***, $p < 0.001$; ****, $p < 0.0001$, analyzed with unpaired *t* test.

various methods were significantly reduced in HepG2 and Huh7 cells lacking NCOA3, whereas overexpression of NCOA3 accelerated Huh7 proliferation and colony formation (Fig. 4, *D–I*). As LPAR6 was down-regulated after *NCOA3* knockdown, we further asked whether compensation of LPAR6 could rescue cell proliferation deficiency caused by NCOA3 depletion. The results showed that LPAR6 overexpression was able to rescue cell proliferation from *NCOA3*-knockdown–induced inhibition in HepG2, Huh7, and SK-Hep1 (Fig. 4*J*). Earlier we showed that U0126 also rescued NCOA3 expression (Fig. 3*G*). These combined results suggest that LPAR6 is transcriptionally regulated by NCOA3, and HGF may inhibit liver cancer proliferation by blocking NCOA3 and LPAR6 expression.

NCOA3 regulates H3K27ac enrichment at LPAR6 locus in response to HGF stimulation

To gain further insights into the role of NCOA3 regulation on LPAR6 expression, we investigated the distribution of histone modifications at the *LPAR6* gene locus. H3K27ac enrichment was remarkably reduced in the *LPAR6* promoter (site 2 and site 3) and coding sequence region (site 1) in *NCOA3*-knockdown cells (Fig. 5, *A* and *B*), whereas H3K9ac, H3K4me3, H3K9me3, and H3K27me3 enrichment was only slightly changed (Fig. S2). The reduced H3K27ac enrichment at the *LPAR6* promoter was not due to diminished H3 expression, because knocking down *NCOA3* did not affect H3 expression (Fig. 4*C*). These results suggest that NCOA3 regulates *LPAR6*

transcription by manipulating H3K27 acetylation in HepG2 cells. The mechanism of NCOA3 regulating H3K27ac enrichment at the LPAR6 locus was similarly replicated in Huh7 cells (Fig. 5*C*).

Because HGF inhibited NCOA3 and LPAR6 expression (Fig. 5*D*), we speculate that HGF may also affect H3K27ac deposition at *LPAR6* locus. As we expected, H3K27ac enrichment at the *LPAR6* promoter (site2 and site3) and coding sequence

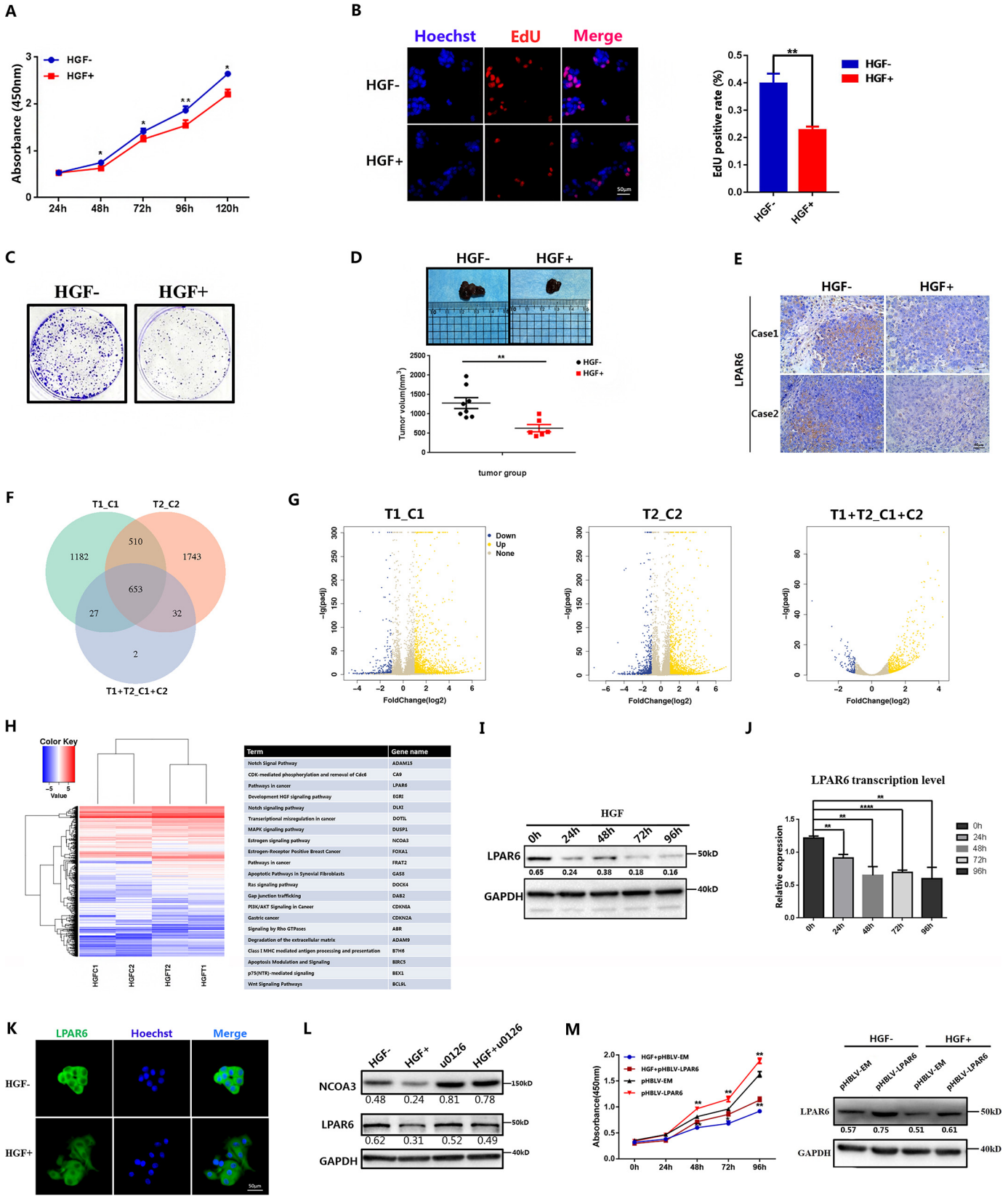

region (site 1) was also significantly reduced in response to HGF treatment in HepG2 and Huh7 cells (Fig. 5, *E* and *F*). H3K36me3 enrichment also showed remarkable reduction at the *LPAR6* coding sequence region (site1), but not at the promoter region (sites 2 and 3, Fig. S3).

Meanwhile, HGF treatment also significantly reduced NCOA3 enrichment at the *LPAR6* loci (sites 1–3, Fig. 5*G*), and the NCOA3 distribution pattern was consistent with H3K27ac. Taken together, these data indicate that HGF-induced down-regulation of *LPAR6* transcription attributes mainly to H3K27ac enrichment reduction at *LPAR6* loci, and partially to the H3K36me3 reduction in the *LPAR6* coding-sequence region (Fig. S3). Generally, acetylation removes positive charges on the histones. As a consequence, the condensed chromatin is transformed into a more relaxed structure that is associated with active transcription. In addition, the gene body marked with H3K36me3 is also associated with active transcription. Therefore, the above results indicate that HGF may regulate transcription by remodeling the chromatin structure to fulfill its anti-tumor function in liver cancer.

The deficiency of LPAR6 and/or NCOA3 limits cell proliferation in vivo

Both *NCOA3* and *LPAR6* knockdown significantly suppresses the growth of HepG2 cells *in vitro*. Therefore, we compared HepG2-derived xenograft tumor growth among the control, *LPAR6*-knockdown, and *NCOA3*-knockdown cells. Either *LPAR6*- or *NCOA3*-knockdown HepG2 cells and control cells ($n = 6$/group) were, respectively, inoculated into the dorsal ventral side of nude mice. After 30 days of growth, the average volume and weight of *LPAR6*-knockdown (sh*LPAR6*) tumors were obviously smaller than those in the control group (NT), suggesting *LPAR6* deficiency affected cell proliferation *in vivo* (Fig. 6*A*). Similarly, the mean volume and weight of tumors with *NCOA3*-knockdown were also much smaller than the control tumors when monitored at Day 20. Given H3K27ac enrichment at the *LPAR6* promoter, these data imply that *LPAR6* requires H3K27ac and NCOA3 to drive proliferation (Fig. 6*B*).

HGF significantly limits liver cancer cell proliferation in vivo

Given that HGF inhibits HepG2 cell proliferation, we speculated that HGF could limit liver cancer cell proliferation *in vivo*. To test this possibility, we generated xenografts with HepG2 cells and cultured them with HGF *in vitro* for 4 days. Twenty-eight days after inoculation, we found that the tumor size and weight were significantly smaller in the HGF-treated group (Fig. 6*C*). EdU staining and apoptosis testing of HepG2 cells suggested that the cells were viable before being implanted into mice (Fig. S4).

To further examine the effect of HGF treatment, we directly injected HGF into the tumors in mice. After treating with HGF for seven times, the mean volume of HGF-treated tumors was smaller (Fig. 6*D*). However, during the treatment period, the mean tumor dimension for the HGF-treated group was slightly larger than the control group (data not shown), which may be due to other HGF-induced physiological functions such as angiogenesis promotion. Therefore, to limit this side effect of HGF on tumor, we carried out a combinatorial treatment with sorafenib, an anti-cancer drug inhibiting vascular endothelial growth factor receptor, platelet-derived growth factor receptor, and Raf family kinases. As we expected, the size and weight of tumors treated with the sorafenib-HGF combined therapy were much smaller than those treated with sorafenib only (Fig. 6*E*).

HGF treatment inhibited LPAR6 expression in liver cancer xenograft

Thus far, our data demonstrated that NCOA3 transcriptionally up-regulated LPAR6 in liver cancer cells, and HGF inhibited LPAR6 expression. However, how HGF signals through NCOA3 to regulate *LPAR6* in liver cancer patients, and whether NCOA3 and LPAR6 function in concert have not yet been fully determined. To this end, we first examined the expression pattern of HGF and LPAR6 in the same patient tumor tissue. Immunohistochemistry (IHC) results suggest that HGF and LPAR6 expression levels were negatively correlated (Fig. 7*A*). Interestingly, our results showed that tumors expressed low levels of HGF, much lower than their matched paracancerous tissues, but high levels of LPAR6 (Fig. 7, *B* and *C*).

Moreover, liver cancer xenograft tumor tissues showed significantly reduced LPAR6 expression in the combined treatment group compared with sorafenib-only group (Fig. 7*D*). The statistical analysis of histochemical indicators showed remarkable LPAR6 reduction in the combined treatment group (Fig. 7*E*). Through the analysis, we also found an HGF expression pattern that is favorable in normal liver tissue instead of tumor tissues (Fig. 7, *F–H*). Considering the remarkable anti-tumor effect of the sorafenib-HGF combination protocol *in vivo*, these results further support that LPAR6 is a potential target of liver cancer.

Figure 3. HGF inhibits LPAR6 expression. *A,* HGF represses HepG2 cell proliferation. Data represents mean ± S.D. The statistical differences were determined by Student's *t* test (*, $p < 0.05$; **, $p < 0.01$). *B, left panel*: EdU staining for cell viability. *Scale bar* = 50 μm. *Right panel*: statistical analysis of EdU-positive cells within the HGF− and HGF+ groups shows decreased proliferation cells in the HGF+ group compared with the HGF− group. *C,* colony formation of HepG2 cells with or without HGF treatment. *D,* tumor xenograft assay showing HGF inhibition of HepG2 cell growth *in vivo*. HepG2 cells pre-treated with HGF (HGF+) or not treated (HGF−) *in vitro* were implanted in 5-week-old nude mice ($n = 8$/HGF−, $n = 6$/HGF+), the volume of xenograft tumors was measured and statistically analyzed (**, $p < 0.01$). *E,* representative IHC slides stained for LPAR6 in xenograft tumors derived from HepG2 cells. *Scale bar* = 50 μm. *F,* Venn diagram showing gene expression in HepG2 cells with or without HGF treatment. *T* and *C* represent HGF-treated cells and untreated control cells, respectively. *G,* differential gene expression distribution using $|\log2(\text{fold-change})| > 2$ and *q*-value < 0.005 as a threshold value for calculation. The DEG analysis was done by Cuffdiff in the Cufflinks package. *Yellow dots* represent up-regulated genes, whereas *blue dots* represent down-regulated genes. *H,* hierarchical clustering analysis for differentially expressed genes indicates that the transcription level of *LPAR6* decreased with HGF treatment. *I,* immunoblotting analysis and *J,* qPCR analysis of LPAR6 expression showing that protein and RNA levels of LPAR6 both reduced in the time course of HGF treatment. GAPDH serves as internal control. *Error bars* represent the S.D. from at least three independent biological replicates (**, $p < 0.01$; ****, $p < 0.0001$). *K,* representative images of immunofluorescent staining of LPAR6 expression with or without HGF treatment. *Scale bar* = 50 μm. *L,* immunoblotting analysis showing that inhibition of the MEK/ERK signal pathway by U0126 rescued LPAR6 expression. *M, left panel*: overexpression of *LPAR6* (pHBLV-LPAR6) promoted cell proliferation compared with control (pHBLV-EM) in HepG2. *Right panel*, immunoblotting validation of LPAR6 expression in HepG2 in the presence or absence of HGF treatment.

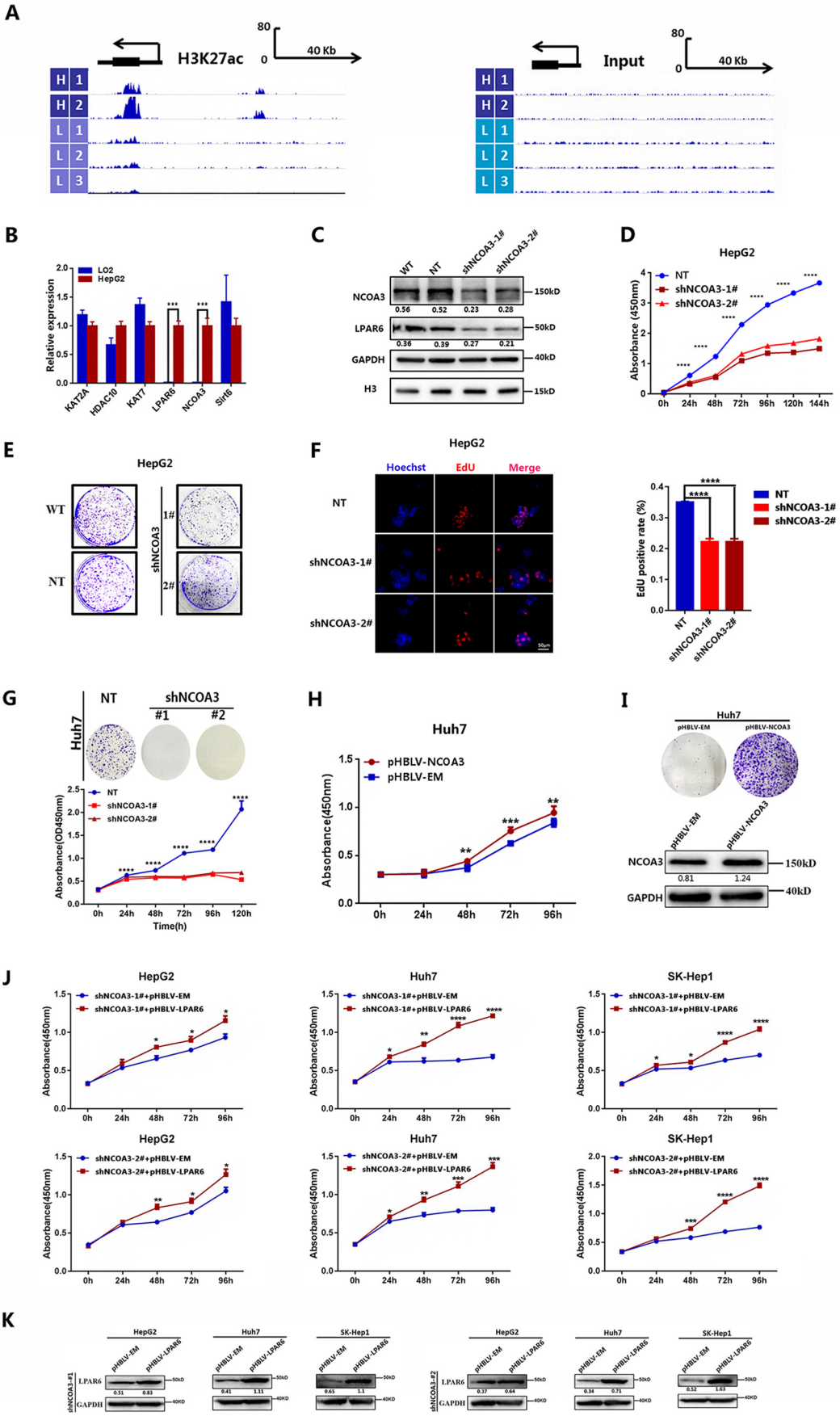
A
H3K27ac
Input
40 Kb
B
Relative expression
LO2
HepG2
KAT2A
HDAC10
KAT7
LPAR6
NCOA3
Sirt6
C
WT
NT
shNCOA3-1#
shNCOA3-2#
NCOA3
LPAR6
GAPDH
H3
150kD
50kD
40kD
15kD
D
HepG2
NT
shNCOA3-1#
shNCOA3-2#
Absorbance (450nm)
E
HepG2
WT
NT
shNCOA3
1#
2#
F
HepG2
Hoechst
EdU
Merge
NT
shNCOA3-1#
shNCOA3-2#
EdU positive rate (%)
G
Huh7
NT
shNCOA3
#1
#2
Absorbance(OD450nm)
Time(h)
H
Huh7
pHBLV-NCOA3
pHBLV-EM
Absorbance(450nm)
I
Huh7
pHBLV-EM
pHBLV-NCOA3
NCOA3
GAPDH
150kD
40kD
J
HepG2
Huh7
SK-Hep1
shNCOA3-1#+pHBLV-EM
shNCOA3-1#+pHBLV-LPAR6
shNCOA3-2#+pHBLV-EM
shNCOA3-2#+pHBLV-LPAR6
Absorbance(450nm)
K
HepG2
Huh7
SK-Hep1
pHBLV-EM
pHBLV-LPAR6
shNCOA3-#1
shNCOA3-#2
LPAR6
GAPDH

Discussion

The development of liver cancer drugs is almost stagnant. Even more frustrating is that the only first-line drug for liver cancer, sorafenib, provides poor benefits. Finding new targets and developing more drugs is necessary but challenging in the area of liver cancer. Here we identified a novel mechanism where HGF exerted the anti-proliferation effect in liver cancer by blocking NCOA3 activity in H3K27 acetylation at the LPAR6 promoter region, leading to down-regulated LPAR6 expression. In addition, the combination of HGF and sorafenib sufficiently inhibited the growth of HepG2-derived xenografts.

Overexpression of HGF in liver cancer models has revealed both tumor-promoting and tumor-inhibiting effects of HGF (16). HGF/Met signaling contributes to tumor angiogenesis, invasiveness, and oncogenesis. Tumor metastasis in many cancer types involves the HGF/Met pathway, leading to the rapid growth of HGF/Met pathway-targeted anticancer drug developmental programs (16, 39). Nonetheless, several studies have also reported that HGF expression is down-regulated in some liver cancer tissues (15, 16). *In vitro* experiments show that HGF can specifically inhibit the growth of HepG2 cells, but no repression effect was observed in Huh7 and SK-Hep1 cells (data not shown) (21, 25). The low repression effect of HGF on SK-Hep1 cells may be due to loss of p53, whereas HepG2 has WT p53. Therefore, these results support the hypothesis that HGF expression is important for liver cancer development and may serve as a potential drug candidate for certain types of liver cancer. Further understanding of the molecular details downstream of the HGF-Met pathway may present additional therapeutic strategies.

LPAR6 is involved in cell growth, motility, and morphological changes (25, 27). By analyzing the data from the TCGA database, we found high expression of LPAR6 in liver cancer ($p < 0.0001$), which was closely related to the poor prognosis of patients ($p < 0.05$). Through IHC staining, we also found that 88% of cancer samples showed high LPAR6 expression compared with paracancerous tissues. This observation is supported by an earlier study reporting that overexpression of LPAR6 in liver cancer specimens was associated with poor survival. Knockdown of LPAR6 inhibit liver cancer cell proliferation by reducing proto-oncogene PIM3 (29).

The HGF-Met signaling pathway plays an essential role in diverse developmental processes, and its dysregulation contributes to metastatic phenotypes of human cancers (40). Our study using liver cancer cell lines demonstrated that LPAR6 and NCOA3 functioned as novel key downstream effectors of the HGF-Met signaling pathway. HGF down-regulates LPAR6, suppressing HepG2 proliferation by arresting the cell cycle at the G1 phase. Our observation supports previous findings that knockdown of *LPAR6* leads to proliferation arrest of liver cancer cell lines, and liver cancer patient tumor tissues with LPAR6 overexpression showed higher proliferative activity (29, 30). These results suggest that LPAR6 is a downstream target of HGF and could serve as a potential therapeutic drug target.

Our study showed that H3K27ac was significantly enriched in the *LPAR6* promoter region in HepG2 cells compared with normal liver cells. Given that the effects of histone acetylation on gene transcription activation are primarily mediated through relaxing the chromatin high order structure to allow transcription factors and RNA polymerases to access gene promoter, we postulated that H3K27ac was a major epigenetic modification involved in the up-regulation of *LPAR6* transcription in liver cancer cells. By screening, we found that *NCOA3* transcription was significantly higher in HepG2 than normal liver cells. As a transcriptional coactivator, NCOA3 has intrinsic HAT activity as well as the capacity of recruiting the CBP/p300-associated factor and CREB-binding protein to form a transcriptional activation complex (34, 41, 42). Our further investigation revealed *NCOA3* knockdown in HepG2 down-regulated LPAR6. Moreover, HepG2 cells treated with HGF showed decreased expressions of NCOA3 and LPAR6 with reduced H3K27ac and H3K36me3 enrichment at *LPAR6* loci. The decreased transcription of *LPAR6* is further confirmed in NCOA3-depleted cells. Together, we show for the first time that HGF down-regulates NCOA3, leading to reduced transcription of *LPAR6* with diminished enrichment of H3K27ac on its promoter locus, thus demonstrating anti-tumorigenesis property.

Currently, sorafenib serves as a first-line anti-liver cancer drug. Therefore, we evaluated the effect of the sorafenib-HGF combination therapy on liver cancer and found that the combinatorial therapy remarkably suppressed the growth of HepG2-derived xenografts. Thus, the HGF-sorafenib combination protocol might be a promising therapeutic strategy for liver cancer patients that have high LPAR6 but low HGF expression. Given the critical role of HGF signaling and the sharing of some downstream signaling components among different growth factor signaling pathways, LPAR6 and NCOA3 may participate in other growth factor signaling pathways beyond the present study. Future investigation of the potential involvement of LPAR6 and NCOA3 in individual growth factor

Figure 4. NCOA3 promotes liver cancer cell proliferation by manipulating LPAR6 expression. *A,* enrichment analysis showing that H3K27ac enrichment at *LPAR6* promoter locus was increased in HepG2 cells compared with normal liver cells. *H,* HepG2 cells; *L,* liver cells. ChIP enrichment results were analyzed from the WashU database. *B,* screening of epigenetic regulators that modulate histone acetylation. The RNA level of NCOA3 is up-regulated in HepG2 cells compared with LO2 liver cells. The indicated RNA level was normalized to the housekeeping gene, *GAPDH*. *Error bars* represent S.D. from at least three independent biological replicates (**, $p < 0.01$; ****, $p < 0.0001$). *C,* verification of *NCOA3* knockdown and LPAR6 expression with or without *NCOA3* knockdown. *D,* knockdown of *NCOA3* inhibited HepG2 cell proliferation (****, $p < 0.0001$). Cell proliferation was measured with CCK8 kit. *E,* colony-formation assay in control and *NCOA3*-knockdown HepG2 cells. The ability of colony formation decreased with NCOA3 depletion compared with NT control. *F, left panel*: EdU staining shows the reduction of cell proliferation after *NCOA3* depletion. Cells were incubated with 50 μM EdU for 2 h. *Scale bar* = 50 μm. *Right panel*: EdU-positive cells were quantified and shown as mean percentage ± S.D. *G,* colony formation and cell-proliferation assays in Huh7 cells with or without *NCOA3* knockdown. *H,* cell-proliferation assay in Huh7 cells with or without *NCOA3* overexpression. *I,* colony-formation assay in Huh7 cells with or without overexpression of *NCOA3*. *J,* overexpression of *LPAR6* elevates cell proliferation in three liver cancer cell lines with NCOA3 depletion. *shNCOA3-1/2#*: lentivirus packaging two different shRNA targeting *NCOA3* gene. *pHBLV-EM*, empty lentivirus. pHBLV-LPAR6: lentivirus encoding *LPAR6*. **, $p < 0.01$; ***, $p < 0.001$; and ****, $p < 0.0001$ by unpaired *t* test. *K,* immunoblotting of LPAR6 expression in three liver cancer cell lines transfected with either pHBLV-EM or pHBLV-LPAR6 lentivirus after NCOA3 depletion.

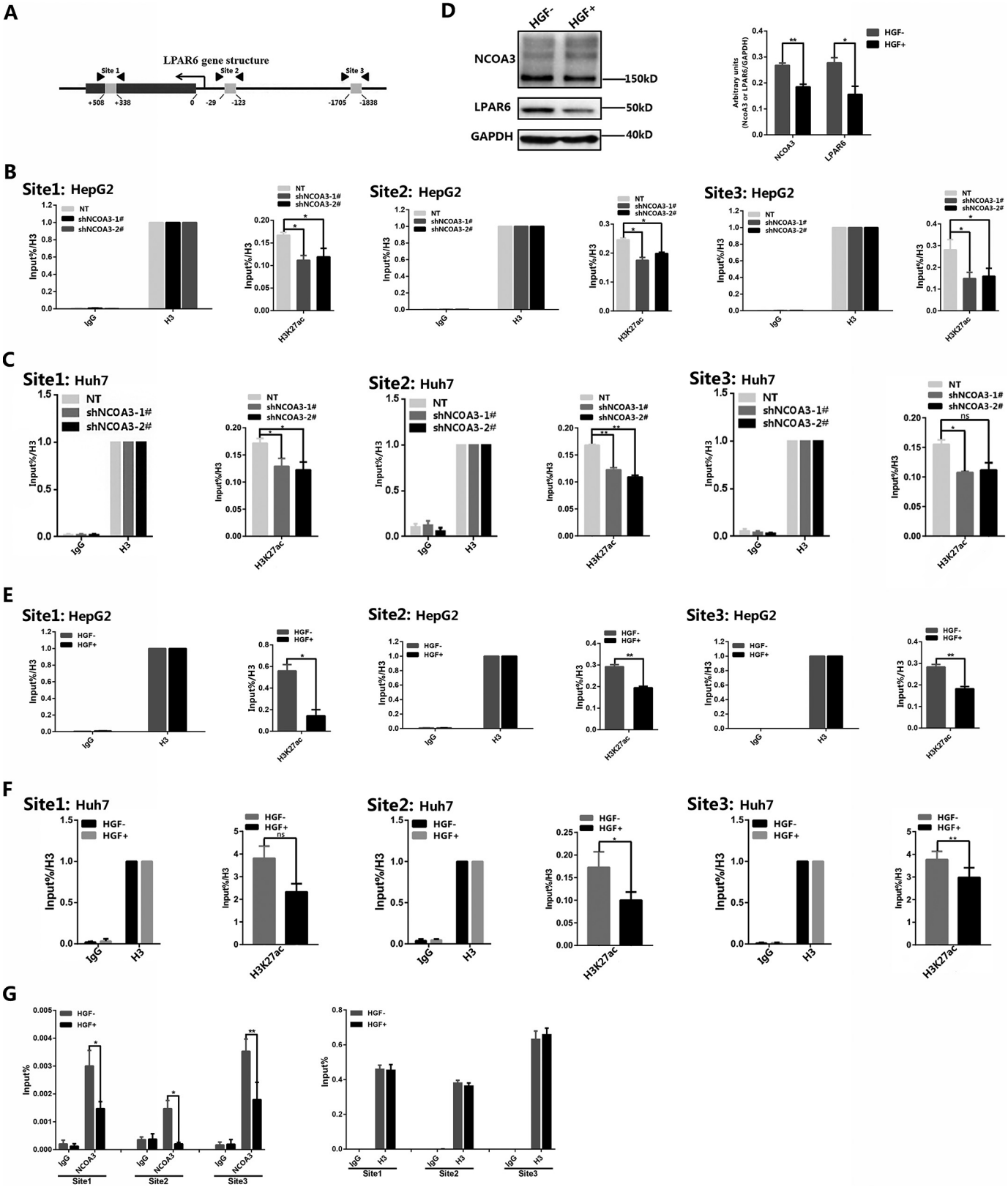
A
LPAR6 gene structure
Site 1
Site 2
Site 3
+508
+338
0
-29
-123
-1705
-1838
D
HGF-
HGF+
NCOA3
LPAR6
GAPDH
150kD
50kD
40kD
Arbitrary units (Ncoa3 or LPAR6/GAPDH)
NCOA3
LPAR6
B
Site1: HepG2
Site2: HepG2
Site3: HepG2
NT
shNCOA3-1#
shNCOA3-2#
Input%/H3
IgG
H3
H3K27ac
C
Site1: Huh7
Site2: Huh7
Site3: Huh7
E
Site1: HepG2
Site2: HepG2
Site3: HepG2
HGF-
HGF+
F
Site1: Huh7
Site2: Huh7
Site3: Huh7
G
Input%
NCOA3
Site1
Site2
Site3

signaling pathways may shed additional light on the anti-cancer effect beyond HGF.

Materials and methods

Cells and cell culture

HepG2, Huh7, and SK-Hep1 cells were purchased from the Cell Bank of the Chinese Academy of Sciences in 2016. Cells were generally passaged less than 5 times, and freshly thawed cells were maintained in culture for no more than 2 weeks before conducting experiments. Cells were routinely tested for mycoplasma contamination using PCR. All cells were cultured in Dulbecco's modified Eagle's medium (HyClone) containing 10% fetal bovine serum (PAN) and 100 units/ml of penicillin/streptomycin (HyClone) at 37 °C in a humidified incubator with 5% CO_2.

Cell-proliferation assay and EdU-staining assay

For the cell-proliferation assay, cells were seeded at a density of 6×10^3/well in 96-well-plates and maintained with HGF for 5 to7 days. Cell proliferation was measured using a CCK8 kit at serial time points as indicated in the figures (Dojindo Laboratories). For the EdU assay, cells were preincubated with 50 μM EdU (RiboBio) for 2 h, and fixed with 4% paraformaldehyde for 30 min and neutralized with 2 mg/ml of glycine. After washing with PBS for three times, cells were stained with Apollo for 30 min. Last, cells were treated with 0.5% Triton X-100 for 10 min and cellular DNA was stained with Hoechst for 10 min. After washing with PBS for three times, images were acquired using Zeiss LSM-710 microscope.

Colony assay and cell cycle analysis

Cells were plated at a density of 1×10^3/well into 6-well-plates, and cultured with Dulbecco's modified Eagle's medium containing 10% fetal bovine serum for 10 days. Cell colonies were detected with crystal violet staining. The photos of colonies were obtained using Molecular Imager Gel Do XR+ system (Bio-Rad). For cell cycle analysis, cells were fixed with 70% ethanol overnight, and digested with trypsin for 30 min at 37 °C before propidium iodide staining (KeyGEN BioTECH). At least 10,000 live cells were subject to FACS analysis on a FACS Calibur flow cytometer (BD Biosciences). Experimental data were analyzed using FlowJo software.

Quantitative real-time PCR primers

Primers used for qPCR are as follows: LPAR6: 5′-TCAGCATGGTGTTTGTGCTTGG-3′ (forward), 5′-CTCCAAATGGCCAATTCCGTGTTG-3′ (reverse); NCOA3: 5′-GTGCTTTGCCCTGTCTCAGC-3′ (forward), 5′-CAGGCCTCATGGAGGATCTCAG-3′ (reverse); GAPDH, 5′-GATTCCACCCATGGCAAATTC-3′ (forward), 5′-CTTCTCCATGGTGGTGAAGAC-3′ (reverse); KAT2A: 5′-GCGGAAATGCATCCTGCAGATG-3′ (forward), 5′-CAGGTGTCTCAAGCTTCCAGTAG-3′ (reverse); KAT7: 5′-CAGTACATGAGACAGGGCTATGGC-3′ (forward), 5′-GGATTCACAGCCGTCTCCTGAC-3′ (reverse); HDAC10: 5′-GCCAACGGGTTCTGTGTGTTC-3′ (forward), 5′-CATGCTCATAGCGGTGCCAG-3′ (reverse); Sirt6: 5′-CCTGGCACTCGCCGATGAG-3′ (forward), 5′-CAGGTGCTTCATGAGCCGG-3′ (reverse).

Quantitative real-time PCR

Total RNA was extracted using TRIzol reagent (ThermoFisher). Briefly, homogenized samples were incubated for 5 min and 0.2 ml of chloroform was added to every milliliter of sample homogenized with TRIzol reagent. After centrifuging at $12,000 \times g$ for 15 min at 4 °C, the aqueous phase was transferred into a new tube with 500 μl of isopropyl alcohol and incubated for 10 min. The pellets were collected by centrifuging at $12,000 \times g$ for 10 min at 4 °C and washed twice with 75% ethanol. The resulted pellets were dissolved in diethyl pyrocarbonate-treated dH_2O for further experiments. Reverse transcription was carried out using the PrimeScript™ RT reagent kit with gDNA Eraser (Takara) according to the manufacturer's protocol. Quantitative PCR using SYBR Green Supermix (Bio-Rad) was performed using CFX96 Real-time PCR System (Bio-Rad).

Virus infection

Lentivirus was packaged with short hairpin RNA targeting LPAR6 and NCOA3. The constructed shRNA plasmids of pLKO.1-LPAR6-puro or pLKO.1-NCOA3-puro were co-transfected with packing plasmids psPAX2 and PMD2.G into 293T cells. The viral supernatants were harvested, pooled, and filtered with 0.45-μm PES membrane filter, and used to infect target cells. The cells were selected with puromycin.

LPAR6-Lentivirus shRNA-1# was 5′-CCGGGACAGAACTTTCAAGTTCCTTCTCGAGAAGGAACTTGAAAGTTCTGTCTTTTT-3′ (forward) and 5′-AATTCAAAAAGACAGAACTTTCAAGTTCCTTCTCGAGAAGGAACTTGAAAGTTCTGTC-3′ (reverse). LPAR6-Lentivirus shRNA-2# was 5′-CCGGGCATTCTGTTCTTAACCTGTACTCGAGTACAGGTTAAGAACAGAATGCTTTTT-3′ (forward) and 5′-AATTCAAAAAGCATTCTGTTCTTAACCTGTACTCGAGTACAGGTTAAGAACAGAATGC-3′ (reverse).

NCOA3-Lentivirus shRNA-1# was 5′-CCGGTTCCACCTCCTAGGGATATAACTCGAGTTATATCCCTAGGAGGTGGAATTTTTG-3′ (forward) and 5′-AATTCAAAAATTCCACCTCCTAGGGATATAACTCGAGTTATATCCCTAGGAGGTGGAA-3′ (reverse). NCOA3-Lentivirus shRNA-2# was 5′-CCGGGGATCAGAAGGCAGGATTATACTCGAGTAT-

Figure 5. NCOA3 regulates H3K27ac enrichment at *LPAR6* locus. *A,* schematic diagram of the *LPAR6* gene and specific primers designed for qPCR. *Black box* represents the CDS region of *LPAR6*; *gray boxes* represent amplification sites by ChIP-qPCR. *B* and *C,* H3K27ac enrichment in (*B*) HepG2 or (*C*) Huh7 cells with or without NCOA3 knockdown. Equal amounts of cells were collected after *NCOA3* shRNA or scrambled shRNA transfection for 48 h and then subject to ChIP. Primers designed for site 1 amplified the *LPAR6*-coding sequence, whereas sites 2 and 3 amplified the *LPAR6* promoter. *Error bars* represent S.D. from three independent biological replicates. *, $p < 0.05$ and **, $p < 0.01$, significance of difference was analyzed by unpaired *t* test. *D,* HGF treatment decreased NCOA3 expression in HepG2 cells. *Bar graph* represents the quantification of immunoblotting bands, with *error bars* representing S.D. of three independent biological replicates. *E* and *F,* HGF remarkably reduced H3K27ac enrichment at *LPAR6* locus in (*E*) HepG2 and (*F*) Huh7 cells. Equal amounts of cells were collected after HGF treatment and then subject to ChIP. *G,* HGF treatment remarkably reduced NCOA3 enrichment at *LPAR6* locus. The specific antibody against NCOA3 was used for immunoprecipitation (*left panel*). Negative control of IgG and positive control of H3 were presented in *right panel*.

AATCCTGCCTTCTGATCCTTTTTG-3′ (forward) and 5′-AATTCAAAAAGGATCAGAAGGCAGGATTATACTCGAGTATAATCCTGCCTTCTGATCC-3′ (reverse).

Immunohistochemistry and immunofluorescence

Specimens of liver cancer tissues were collected for IHC analysis of LPAR6 and HGF. Antibodies to LPAR6

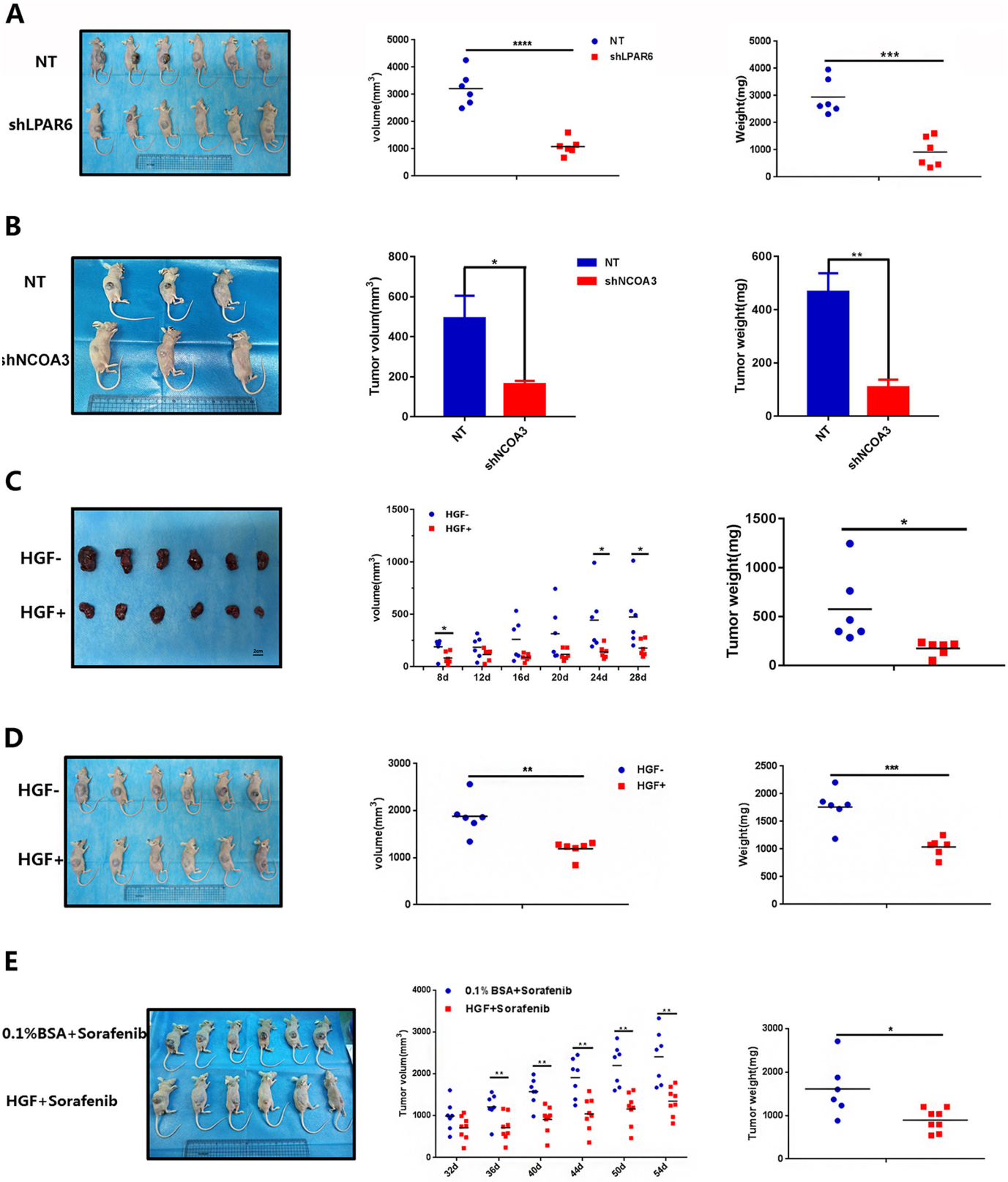

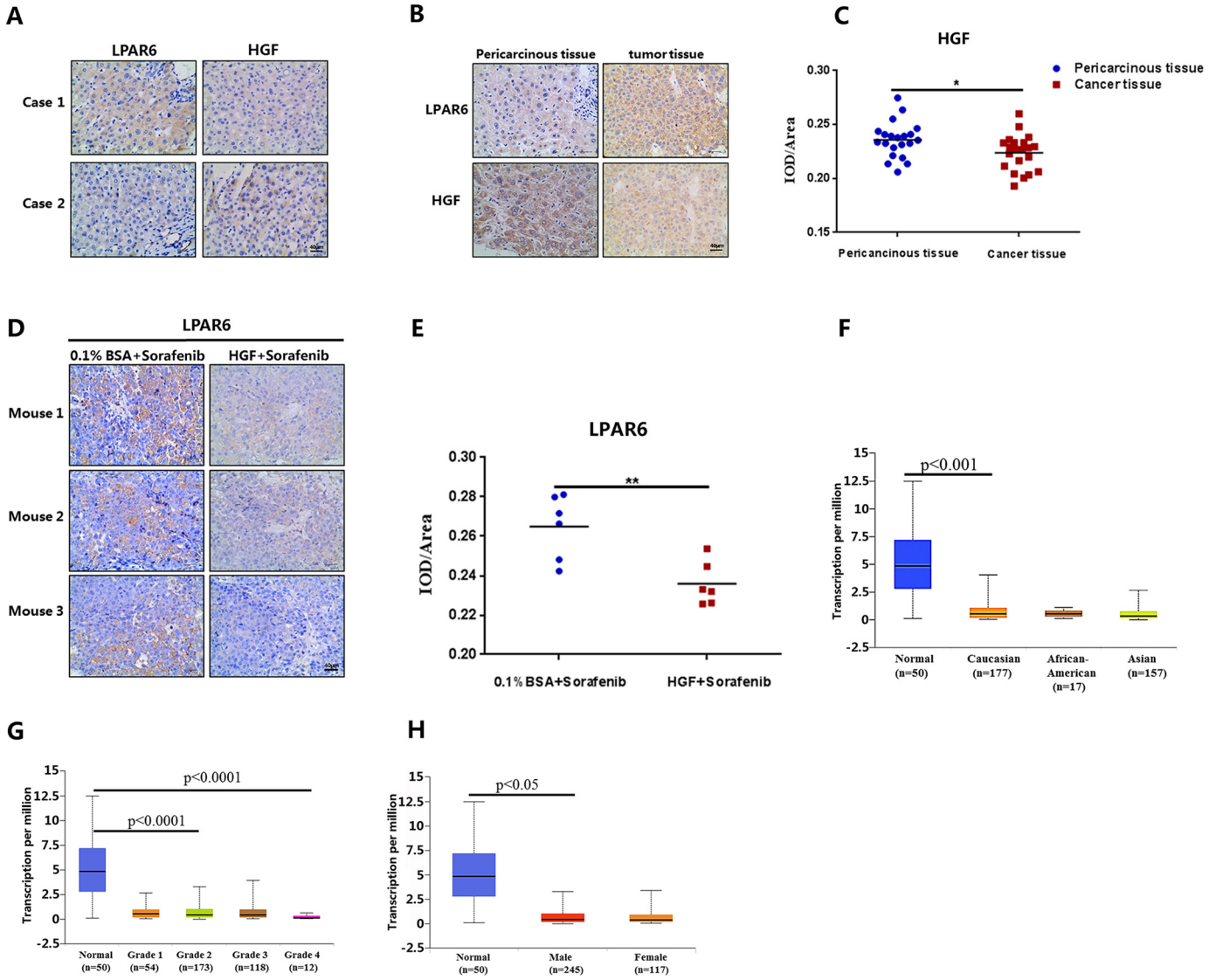

Figure 7. Correlation analysis of LPAR6 and HGF in liver cancer patients and HepG2 cell-derived xenograft tissues. *A,* LPAR6 expression is negatively correlated with HGF expression in human liver cancer tissues. *B* and *C,* LPAR6 or HGF staining and statistical analysis in paracancerous and tumor tissue. Immunostaining of HGF was scored with IOD/area. *D,* LPAR6 expression in xenograft treated with HGF only or HGF-sorafenib combined therapy. *E,* quantification of LPAR6 expression with (IOD)/area in xenograft after treatment. *F–H,* analysis of HGF expression in liver cancer patients based on race, tumor grade, and patient gender.

(ab135447) and HGF (ab83760) were purchased from Abcam. For immunofluorescence analysis, the prepared cells were fixed with 4% paraformaldehyde and blocked with PBS containing 1% BSA and 0.1% Triton X-100. Slides were incubated with primary antibodies overnight at 4 °C. Following four washes with 0.1% BSA/PBS/Triton X-100, cells were incubated with fluorescein-conjugated secondary antibody for 1 h at room temperature. After four washes, cells were stained with 0.1 μg/ml of 4′,6-diamidino-2-phenylindole in PBS for 15 min at room temperature followed by two washes with PBS. Images were acquired using Zeiss microscope.

Figure 6. LPAR6/NCOA3 depletion or HGF-sorafenib combination significantly inhibits xenografts growth. *A,* LPAR6 loss represses xenograft growth. HepG2 cells were infected with lentivirus containing shRNA against *LPAR6* or nontargeting scrambled shRNA. After knockdown validation with immunoblotting, infected cells were implanted into the dorsal flanks of 5-week-old nude mice (*NT*, $n = 6$; *shLPAR6*, $n = 6$). After 30 days, we analyzed xenograft tumor volume and tumor weight. *p* value was analyzed with unpaired *t* test (***, $p < 0.001$). *B, NCOA3* knockdown represses xenograft growth. Cell infection and implantation procedures were conducted as described in *A* (*NT*, $n = 3$; *shNCOA3*, $n = 3$). After 20 days, xenograft tumor volume and weight were analyzed. Data represent mean ± S.D. *, $p < 0.05$ and **, $p < 0.01$, analyzed with unpaired *t* test. *C,* pre-treatment with HGF delayed xenograft tumor formation. HepG2 cells cultured with or without HGF treatment for 4 days, and then the same number of cells (HGF- *versus* HGF+) were implanted into the dorsal flanks of 5-week-old nude mice for 28 days and monitored (HGF−, $n = 6$; HGF+, $n = 6$). *, $p < 0.05$, analyzed with unpaired *t* test. *D,* HGF treatment inhibited xenograft tumor growth. HepG2-derived xenograft mice were divided into two groups based on similar tumor size (HGF−, $n = 6$; HGF+, $n = 6$), and then subjected to intratumoral injection of HGF continuously for 7 days. Control was intratumorally injected with 0.1% BSA as a same volume with HGF. Tumor growth was monitored for 30 days, and xenograft tumor volume and weight were analyzed at the end point. **, $p < 0.01$; ***, $p < 0.001$. *E,* xenograft mice were generated as described in *D* and then treated with either sorafenib-only or HGF-sorafenib combined therapy (HGF−, $n = 6$; HGF+, $n = 6$) for 10 days. Tumor growth was monitored for 54 days. *, $p < 0.05$ and **, $p < 0.01$, analyzed with unpaired *t* test.

RNA-seq library preparation and data analysis

Briefly, mRNA purified from total RNA using poly(A) selection was chemically fragmented and converted into single-stranded cDNA using random hexamer priming. Double-stranded (ds) cDNA was generated for TruSeq library construction. Short ds-cDNA fragments were linked with sequencing adapters, and suitable fragments were separated by agarose gel electrophoresis. Constructed TruSeq RNA libraries were quantified using quantitative PCR, and the quality was assessed by electrophoresis (Bioanalyzer 2100, Agilent Technologies). To analyze sequencing data, the transcript counts for gene expression levels were calculated and the relative transcript abundance was determined as fragments per kilobase of exon per million fragments mapped (FPKM) using Cufflinks software. Raw data were extracted as FPKM values across all samples, and samples with zero values across more than 50% of the genes were excluded.

ChIP assay

The ChIP assay was carried out following the protocol described previously (38). Briefly, genomic DNA was sheared by sonication to 300–500 bp. One-sixth of sheared DNA/protein complex lysate was kept as an input. Antibodies against H3 (ab1791), H3K9me3 (ab8898), H3K27me3 (ab6002), H3K36me3 (ab9050), H3K9ac (ab4441), and H3K27ac (ab4729) were purchased from Abcam. Antibody against NCOA3 (20032-1-AP) was purchased from Proteintech. Antibodies against H3K4me3 (07-473) and normal rabbit IgG (12-370) were purchased from Millipore. Enrichment of each antibody at the *LPAR6* locus was evaluated by real-time PCR, and calculated as percentage of input. Primers specific for ChIP are listed: LPAR6–1: 5′-CAAAGCAGGCTTCTGAGGCATTG-3′ (forward), 5′-TCGATTTCTGGCAATTGTCTACCC-3′ (reverse); LPAR6–2: 5′-AGGCACGTCCAATTTTCAGTTTGG-3′ (forward), 5′-ACCATCCAAAGATCCAGATAATTTGC-3′ (reverse); LPAR6–3: 5′-CCTGAGATCAGGAGTTTGAGAGCAG-3′ (forward), 5′-GATTCTCCTGCCTCAGTCTCCTG-3′ (reverse).

Animal study

All animal procedures were performed with respect to the national and international Guidelines for the Care and Use of Laboratory, and also were approved by the Institutional Animal Care and Use Committee from Sichuan University. Four-week-old male Balb/c nude mice and NOD/SCID mice were purchased from Vital River Laboratory Animal Technology Co., Ltd (Beijing). The mice were housed under standard conditions. Mice were administered under pathogen-free conditions.

Tumor-xenograft assay

All animal procedures were performed with respect to the national and international Guidelines for the Care and Use of Laboratory Animals, and also were approved by the local Institutional Animal Care and Use Committee. Cells containing shLPAR6, shNCOA3, or control shRNA were implanted at a density of 9×10^6 cells per mouse into the dorsal ventral side of 5-week-old nude mice, each with the same amount of Matrigel (Corning). Neoplasms were monitored for nearly 2 months. HepG2-derived xenograft nude mice were divided into two groups based on the tumor size 2 weeks post-implantation. HGF with or without sorafenib was injected into tumors once per day for a total of 10 days, compared with 0.1% BSA (with or without sorafenib) injection, respectively. All the mice were housed and supplied with water and food *ad libitum*. Tumor volumes (mm^3) were calculated with the following equation: volume = (length × width^2)/2.

Database and statistical analysis

Analysis of liver cancer specimens were carried out using Ualcan (http://ualcan.path.uab.edu/analysis.html)[4] and TCGA (https://cancergenome.nih.gov/). ChIP enrichment was analyzed with WashU (http://epigenomegateway.wustl.edu/)[4] and ENCODE (https://www.encodeproject.org/)[4] (43). Error bars represent the mean ± S.D. of at least three independent replicates. Statistical significance was evaluated by two-tailed paired Student's *t* test. For correlations, Pearson's *r* coefficients were utilized, and Kaplan-Meier solution was used to assess survival curves. Images of IHC were scored using Image-Pro Plus 6.0 (Media Cybernetics).

Author contributions—X. Zheng and J. H. conceptualization; X. Zheng and J. H. resources; X. Zheng, X. Zeng, and J. H. data curation; X. Zheng, L. X., M. W., C. H., and C. L. formal analysis; X. Zheng and Y. J. investigation; X. Zheng, L. Q., C. H., and C. L. visualization; X. Zheng and J. H. methodology; X. Zheng writing-original draft; L. C. and J. H. supervision; L. C. and J. H. writing-review and editing; J. H. funding acquisition; J. H. project administration.

Acknowledgments—We are grateful to the Core facility of West China Hospital for their support, and Dr. Toshiaki Tanaka for personal communications and providing HGF. We also thank all financial supporters, and Drs. Da Jia, Yong Peng, and Dong Fang for discussions and critical reading.

References

1. Llovet, J. M., Zucman-Rossi, J., Pikarsky, E., Sangro, B., Schwartz, M., Sherman, M., and Gores, G. (2016) Hepatocellular carcinoma. *Nat. Rev. Dis. Primers* **2,** 16018 CrossRef Medline
2. Greten, T. F., and Sangro, B. (2018) Targets for immunotherapy of liver cancer. *J. Hepatol.* **68,** 157–166 CrossRef
3. Cheng, A.-L., Kang, Y.-K., Chen, Z., Tsao, C.-J., Qin, S., Kim, J. S., Luo, R., Feng, J., Ye, S., Yang, T.-S., *et al.* (2009) Efficacy and safety of sorafenib in patients in the Asia-Pacific region with advanced hepatocellular carcinoma: a phase III randomised, double-blind, placebo-controlled trial. *Lancet Oncol.* **10,** 25–34 CrossRef Medline
4. El-Khoueiry, A. B., Sangro, B., Yau, T., Crocenzi, T. S., Kudo, M., Hsu, C., Kim, T.-Y., Choo, S.-P., Trojan, J., Welling, T. H., *et al.* (2017) Nivolumab in patients with advanced hepatocellular carcinoma (CheckMate 040): an open-label, non-comparative, phase 1/2 dose escalation and expansion trial. *Lancet* **389,** 2492–2502 CrossRef Medline
5. Johnson, P. J., Qin, S., Park, J.-W., Poon, R. T., Raoul, J.-L., Philip, P. A., Hsu, C.-H., Hu, T.-H., Heo, J., and Xu, J. (2013) Brivanib *versus* sorafenib as first-line therapy in patients with unresectable, advanced hepatocellular

[4] Please note that the JBC is not responsible for the long-term archiving and maintenance of this site or any other third party hosted site.

carcinoma: results from the randomized phase III BRISK-FL study. *J. Clin. Oncol.* **31,** 3517–3524 CrossRef Medline
6. Stoker, M., Gherardi, E., Perryman, M., and Gray, J. (1987) Scatter factor is a fibroblast-derived modulator of epithelial cell mobility. *Nature* **327,** 239–242 CrossRef Medline
7. Cecchi, F., Pajalunga, D., Fowler, C. A., Uren, A., Rabe, D. C., Peruzzi, B., Macdonald, N. J., Blackman, D. K., Stahl, S. J., Byrd, R. A., and Bottaro, D. P. (2012) Targeted disruption of heparan sulfate interaction with hepatocyte and vascular endothelial growth factors blocks normal and oncogenic signaling. *Cancer Cell* **22,** 250–262 CrossRef Medline
8. Joosten, S. P., Zeilstra, J., van Andel, H., Mijnals, R. C., Zaunbrecher, J., Duivenvoorden, A. A. M., van de Wetering, M., Clevers, H., Spaargaren, M., and Pals, S. T. (2017) MET signaling mediates intestinal crypt-villus development, regeneration, and adenoma formation and is promoted by stem cell CD44 isoforms. *Gastroenterology* **153,** 1040–1053.e4 CrossRef Medline
9. Ma, H., Calderon, T. M., Kessel, T., Ashton, A. W., and Berman, J. W. (2003) Mechanisms of hepatocyte growth factor-mediated vascular smooth muscle cell migration. *Circ. Res.* **93,** 1066–1073 CrossRef Medline
10. Song, K. H., Ellis, E., Strom, S., and Chiang, J. Y. (2007) Hepatocyte growth factor signaling pathway inhibits cholesterol 7α-hydroxylase and bile acid synthesis in human hepatocytes. *Hepatology* **46,** 1993–2002 CrossRef Medline
11. Bauer, T. W., Somcio, R. J., Fan, F., Liu, W., Johnson, M., Lesslie, D. P., Evans, D. B., Gallick, G. E., and Ellis, L. M. (2006) Regulatory role of c-Met in insulin-like growth factor-I receptor-mediated migration and invasion of human pancreatic carcinoma cells. *Mol. Cancer Ther.* **5,** 1676–1682 CrossRef Medline
12. Engelman, J. A., Zejnullahu, K., Mitsudomi, T., Song, Y., Hyland, C., Park, J. O., Lindeman, N., Gale, C.-M., Zhao, X., Christensen, J., *et al.* (2007) MET amplification leads to gefitinib resistance in lung cancer by activating ERBB3 signaling. *Science* **316,** 1039–1043 CrossRef Medline
13. Ponzo, M. G., Lesurf, R., Petkiewicz, S., O'Malley, F. P., Pinnaduwage, D., Andrulis, I. L., Bull, S. B., Chughtai, N., Zuo, D., Souleimanova, M., *et al.* (2009) Met induces mammary tumors with diverse histologies and is associated with poor outcome and human basal breast cancer. *Proc. Natl. Acad. Sci. U.S.A.* **106,** 12903–12908 CrossRef Medline
14. Shojaei, F., Lee, J. H., Simmons, B. H., Wong, A., Esparza, C. O., Plumlee, P. A., Feng, J., Stewart, A. E., Hu-Lowe, D. D., and Christensen, J. G. (2010) HGF/c-Met acts as an alternative angiogenic pathway in sunitinib-resistant tumors. *Cancer Res.* **70,** 10090–10100 CrossRef Medline
15. Giordano, S., and Columbano, A. (2014) Met as a therapeutic target in HCC: facts and hopes. *J. Hepatol.* **60,** 442–452 CrossRef Medline
16. Goyal, L., Muzumdar, M. D., and Zhu, A. X. (2013) Targeting the HGF/c-MET pathway in hepatocellular carcinoma. *Clin. Cancer Res.* **19,** 2310–2318 CrossRef Medline
17. Tavian, D., De Petro, G., Benetti, A., Portolani, N., Giulini, S. M., and Barlati, S. (2000) u-PA and c-MET mRNA expression is coordinately enhanced while hepatocyte growth factor mRNA is down-regulated in human hepatocellular carcinoma. *Int. J. Cancer* **87,** 644–649 CrossRef Medline
18. Han, J., Tsukada, Y., Hara, E., Kitamura, N., and Tanaka, T. (2005) Hepatocyte growth factor induces redistribution of p21(CIP1) and p27(KIP1) through ERK-dependent p16(INK4a) up-regulation, leading to cell cycle arrest at G1 in HepG2 hepatoma cells. *J. Biol. Chem.* **280,** 31548–31556 CrossRef Medline
19. Kondo, A., Hirayama, N., Sugito, Y., Shono, M., Tanaka, T., and Kitamura, N. (2008) Coupling of Grb2 to Gab1 mediates hepatocyte growth factor-induced high intensity ERK signal required for inhibition of HepG2 hepatoma cell proliferation. *J. Biol. Chem.* **283,** 1428–1436 CrossRef Medline
20. Li, X., Bian, Y., Takizawa, Y., Hashimoto, T., Ikoma, T., Tanaka, J., Kitamura, N., Inagaki, Y., Komada, M., and Tanaka, T. (2013) ERK-dependent downregulation of Skp2 reduces Myc activity with HGF, leading to inhibition of cell proliferation through a decrease in Id1 expression. *Mol. Cancer Res.* **11,** 1437–1447 CrossRef Medline
21. Tsukada, Y., Miyazawa, K., and Kitamura, N. (2001) High intensity ERK signal mediates hepatocyte growth factor-induced proliferation inhibition of the human hepatocellular carcinoma cell line HepG2. *J. Biol. Chem.* **276,** 40968–40976 CrossRef Medline
22. Liu, M.-L., Mars, W. M., and Michalopoulos, G. K. (1995) Hepatocyte growth factor inhibits cell proliferation *in vivo* of rat hepatocellular carcinomas induced by diethylnitrosamine. *Carcinogenesis* **16,** 841–843 CrossRef Medline
23. Santoni-Rugiu, E., Preisegger, K. H., Kiss, A., Audolfsson, T., Shiota, G., Schmidt, E. V., and Thorgeirsson, S. S. (1996) Inhibition of neoplastic development in the liver by hepatocyte growth factor in a transgenic mouse model. *Proc. Natl. Acad. Sci. U.S.A.* **93,** 9577–9582 CrossRef Medline
24. Tajima, H., Matsumoto, K., and Nakamura, T. (1991) Hepatocyte growth factor has potent anti-proliferative activity in various tumor cell lines. *FEBS Lett.* **291,** 229–232 CrossRef Medline
25. Kihara, Y., Maceyka, M., Spiegel, S., and Chun, J. (2014) Lysophospholipid receptor nomenclature review: IUPHAR review 8. *Br. J. Pharmacol.* **171,** 3575–3594 CrossRef Medline
26. Yanagida, K., Masago, K., Nakanishi, H., Kihara, Y., Hamano, F., Tajima, Y., Taguchi, R., Shimizu, T., and Ishii, S. (2009) Identification and characterization of a novel lysophosphatidic acid receptor, p2y5/LPA6. *J. Biol. Chem.* **284,** 17731–17741 CrossRef Medline
27. Pasternack, S. M., von Kügelgen, I., Al Aboud, K., Lee, Y., Rüschendorf, F., Voss, K., Hillmer, A., Molderings, G. J., Franz, T., Ramirez, A., Nürnberg, P., Nöthen, M. M., and Betz, R. C. (2008) G protein-coupled receptor P2Y5 and its ligand LPA are involved in maintenance of human hair growth. *Nat. Genet.* **40,** 329–334 CrossRef Medline
28. Shimomura, Y., Wajid, M., Ishii, Y., Shapiro, L., Petukhova, L., Gordon, D., and Christiano, A. (2008) Disruption of P2RY5, an orphan G protein-coupled receptor, underlies autosomal recessive woolly hair. *Nat. Genet.* **40,** 335–339 CrossRef Medline
29. Mazzocca, A., Dituri, F., De Santis, F., Filannino, A., Lopane, C., Betz, R. C., Li, Y., Mukaida, N., Winter, P., Tortorella, C., Giannelli, G., and Sabbà, C. (2015) Lysophosphatidic acid receptor LPAR6 supports the tumorigenicity of hepatocellular carcinoma. *Cancer Res.* **75,** 532–543 CrossRef Medline
30. Sokolov, E., Eheim, A. L., Ahrens, W. A., Walling, T. L., Swet, J. H., McMillan, M., Simo, K. A., Thompson, K. J., Sindram, D., and McKillop, I. H. (2013) Lysophosphatidic acid receptor expression and function in human hepatocellular carcinoma. *J. Surg. Res.* **180,** 104–113 CrossRef Medline
31. Zhou, G., Hashimoto, Y., Kwak, I., Tsai, S. Y., and Tsai, M.-J. (2003) Role of the steroid receptor coactivator SRC-3 in cell growth. *Mol. Cell. Biol.* **23,** 7742–7755 CrossRef Medline
32. Gojis, O., Rudraraju, B., Gudi, M., Hogben, K., Sousha, S., Coombes, R. C., Cleator, S., and Palmieri, C. (2010) The role of SRC-3 in human breast cancer. *Nat. Rev. Clin. Oncol.* **7,** 83–89 CrossRef Medline
33. Xu, J., Wu, R. C., and O'Malley, B. W. (2009) Normal and cancer-related functions of the p160 steroid receptor co-activator (SRC) family. *Nat. Rev. Cancer* **9,** 615–630 CrossRef Medline
34. Chen, H., Lin, R. J., Schiltz, R. L., Chakravarti, D., Nash, A., Nagy, L., Privalsky, M. L., Nakatani, Y., and Evans, R. M. (1997) Nuclear receptor coactivator ACTR is a novel histone acetyltransferase and forms a multimeric activation complex with P/CAF and CBP/p300. *Cell* **90,** 569–580 CrossRef Medline
35. Wang, Y., Lonard, D. M., Yu, Y., Chow, D.-C., Palzkill, T. G., and O'Malley, B. W. (2011) Small molecule inhibition of the steroid receptor coactivators, SRC-3 and SRC-1. *Mol. Endocrinol.* **25,** 2041–2053 CrossRef Medline
36. Juric, V., Ruffell, B., Evason, K. J., Hu, J., Che, L., Wang, L., Chen, X., and Bishop, J. M. (2016) Monocytes promote liver carcinogenesis in an oncogene-specific manner. *J. Hepatol.* **64,** 881–890 CrossRef Medline
37. Xue, W., Krasnitz, A., Lucito, R., Sordella, R., Vanaelst, L., Cordon-Cardo, C., Singer, S., Kuehnel, F., Wigler, M., Powers, S., Zender, L., and Lowe, S. (2008) DLC1 is a chromosome 8p tumor suppressor whose loss promotes hepatocellular carcinoma. *Genes Dev.* **22,** 1439–1444 CrossRef Medline
38. Han, J., Zhou, H., Li, Z., Xu, R.-M., and Zhang, Z. (2007) Acetylation of lysine 56 of histone H3 catalyzed by RTT109 and regulated by ASF1 is required for replisome integrity. *J. Biol. Chem.* **282,** 28587–28596 CrossRef Medline
39. De Silva, D. M., Roy, A., Kato, T., Cecchi, F., Lee, Y. H., Matsumoto, K., and Bottaro, D. P. (2017) Targeting the hepatocyte growth factor/Met

pathway in cancer. *Biochem. Soc. Trans.* **45,** 855–870 CrossRef Medline

40. Birchmeier, C., Birchmeier, W., Gherardi, E., and Vande Woude, G. (2003) Met, metastasis, motility and more. *Nat. Rev. Mol. Cell Biol.* **4,** 915–925 CrossRef Medline
41. Wu, Z., Yang, M., Liu, H., Guo, H., Wang, Y., Cheng, H., and Chen, L. (2012) Role of nuclear receptor coactivator 3 (Ncoa3) in pluripotency maintenance. *J. Biol. Chem.* **287,** 38295–38304 CrossRef Medline
42. Yi, P., Wang, Z., Feng, Q., Chou, C. K., Pintilie, G. D., Shen, H., Foulds, C. E., Fan, G., Serysheva, I., Ludtke, S. J., Schmid, M. F., Hung, M. C., Chiu, W., and O'Malley, B. W. (2017) Structural and functional impacts of ER coactivator sequential recruitment. *Mol. Cell* **67,** 733–743 CrossRef Medline
43. ENCODE Project Consortium. (2012) An integrated encyclopedia of DNA elements in the human genome. *Nature* **489,** 57–74 CrossRef Medline